Kinetic Mechanisms of Inhibitor Binding: Relevance to the Fast-Acting Slow-Binding Paradigm

Said Falk, Nathalie Oulianova, and Alfred Berteloot
Membrane Transport Research Group, Department of Physiology, Faculty of Medicine, Université de Montréal, CP 6128, succursale Centre-Ville, Montreal, Québec H3C 3J7, Canada.

ABSTRACT Although phlorizin inhibition of Na^+-glucose cotransport occurs within a few seconds, ^{3}H-phlorizin binding to the sodium-coupled glucose transport protein(s) requires several minutes to reach equilibrium (the fast-acting slow-binding paradigm). Using kinetic models of arbitrary dimension that can be reduced to a two-state diagram according to Cha's formalism, we show that three basic mechanisms of inhibitor binding can be identified whereby the inhibitor binding step either (A) represents, (B) precedes, or (C) follows the rate-limiting step in a binding reaction. We demonstrate that each of mechanisms A–C is associated with a set of unique kinetic properties, and that the time scale over which one may expect to observe mechanism C is conditioned by the turnover number of the catalytic cycle. In contrast, mechanisms A and B may be relevant to either fast-acting or slow-binding inhibitors. However, slow-binding inhibition according to mechanism A may not be compatible with a fast-acting behavior on the steady-state time scale of a few seconds. We conclude that the recruitment hypothesis (mechanism C) cannot account for slow phlorizin binding to the sodium-coupled glucose transport protein(s), and that mechanism B is the only alternative that may explain the fast-acting slow-binding paradigm.

INTRODUCTION

Competitive inhibitors with specificity for a target protein are useful probes of the kinetic mechanisms of enzyme-catalyzed reactions and membrane transport processes. The general approach to the study of such protein-inhibitor interactions involves the analysis of the decrease in reaction velocity that occurs in the presence of inhibitor as compared to inhibitor-free control conditions. Alternatively, a more direct approach relies on the interpretation of the kinetics of inhibitor binding, usually measured using radiolabeled inhibitors in the presence of some or all of the physiological effectors. In practice, the general approach has mostly been restricted to enzyme reactions for which linear rates of product formation can be measured on a time scale of seconds to minutes in the absence of inhibitor (Morrison and Walsh, 1988). By contrast, the direct approach has been widely applied to a number of transport systems on the rationale that the kinetic equations accounting for inhibitor binding are usually simpler and easier to test than those derived for substrate uptake because fewer carrier forms and translocation steps need to be considered (Turner and Silverman, 1980).

The current concepts describing the reversible interactions between a competitive inhibitor (I) and its target protein have been established within the context of steady-state kinetics of unireactant enzymes (E). These theoretical studies involved the analysis of an elementary reaction scheme in which the formation of the enzyme–substrate complex (ES) is rapid (rapid equilibrium assumption) whereas the overall rate of catalysis is limited by the breakdown of this complex to form product (Morrison and Walsh, 1988). Accordingly, the reaction rate is linear over the time period during which the initial rate assumptions are satisfied (see Note 1). Competitive inhibitors for S are usually referred to as classical or slow-binding inhibitors, defined where the rates of association with and dissociation from E are fast or slow, respectively, relative to the reaction velocity (Morrison and Walsh, 1988). In the presence of classical inhibitors, a steady-state concentration of EI is also rapidly established and the initial rate remains linear, hence their apparent fast-acting behavior. In contrast, the reaction rates in the presence of slow-binding inhibitors demonstrate an initial burst of high reaction rate followed by a slow decrease to a lower steady-state level. Two kinetic mechanisms have been proposed that may account for slow-binding inhibition (Morrison and Walsh, 1988). In mechanism A, the inhibitor binding step itself represents the overall rate-limiting step in the interaction because of barriers that the inhibitor encounters when binding at the active site of the enzyme. For mechanism B, it is assumed that inhibitor binding involves the rapid formation of an initial collision complex, but is followed by a slow isomerization reaction. The burst kinetics described above thus reflect the slow establishment of either the equilibrium between E, I, and EI (mechanism A), or between the two enzyme-inhibitor complexes (mechanism B).

It should be emphasized that the distinction between fast-acting and slow-binding inhibitors is in no way the result of these mechanistic considerations (see Note 2) but simply rests on the assumption that the two classes of inhibitors can be identified through the application of steady-state kinetic methods. Therefore, an obvious limita-

Received for publication 11 May 1998 and in final form 15 April 1999.

Address reprint requests to Dr. Alfred Berteloot, Membrane Transport Research Group, Department of Physiology, Faculty of Medicine, Université de Montréal, CP 6128, succursale Centre-Ville, Montréal, Québec H3C 3J7, Canada. Tel.: 514-343-5634; Fax: 514-343-2111; E-mail: Alfred.Berteloot@umontreal.ca.

0006-3495/99/07/173/16 $2.00

tion to the steady-state formalism is that these methods may fail to detect the occurrence of slow-binding inhibition if the time required to achieve equilibrium binding is much larger than the time period over which the initial rate assumptions are satisfied (see Note 3). Such a limitation is particularly relevant to membrane transport processes for which it may prove difficult to record linear initial rates of transport using isolated membrane preparations or cells for time periods in excess of a few seconds (Berteloot and Semenza, 1990; Chenu and Berteloot, 1993; Kimmich, 1990). This problem is best illustrated by phlorizin, a reversible and highly selective competitive inhibitor of the sodium-coupled glucose transport (SGLT) systems of intestinal and renal tissues, that is not transported by the SGLT proteins (Diedrich, 1966; Aronson, 1978; Semenza et al., 1984; Kimmich, 1990; Wright, 1993). Using a fast-sampling rapid-filtration apparatus (Berteloot et al., 1991) and rabbit renal brush-border membrane vesicles, our recent studies demonstrated that the initial period during which glucose transport rates are constant occurs on a time scale of 0–9 s in the presence or absence of phlorizin (Oulianova and Berteloot, 1996). According to the steady-state formalism, these results should suffice to classify phlorizin as a fast-acting (classical) inhibitor, in which case, one would expect to observe constant binding of labeled inhibitor over a time period during which steady-state reaction rates are recorded (see Note 4). This prediction clearly conflicts with the slow rates of phlorizin binding usually reported using similar preparations, where up to 5 min incubation with radiolabeled phlorizin may be required to reach equilibrium (Glossmann and Neville, 1972; Chesney et al., 1974; Aronson, 1978; Turner and Silverman, 1981; Koepsell et al., 1990). This situation will be referred to as the fast-acting slow-binding paradigm in the present paper.

The current hypothesis for the slow binding of phlorizin is the recruitment concept (referred to as mechanism C in this text), whereby the inhibitor is titrating a carrier conformation in which a substrate binding site becomes accessible to the inhibitor molecules (Aronson, 1978). More precisely, it is proposed that the sugar (phlorizin) binding site on the carrier has a predominant inward orientation, which is therefore shielded from access. A slow translocation (conformational change) to an outward-facing configuration would then explain the slow kinetics of phlorizin binding to this newly available site. To our knowledge, no theoretical justification has ever been provided to support the validity of the recruitment concept, which rests primarily on circumstantial pieces of evidence (Aronson, 1978; Toggenburger et al., 1978, 1982; Turner and Silverman, 1981; Restrepo and Kimmich, 1986). Moreover, the kinetics of phlorizin binding have never been considered with regard to the applicability of mechanisms A and B discussed above. In this respect, it should be noted that the early studies of Turner and Silverman (1980) were only concerned with the kinetics of inhibitor binding at equilibrium. Because all of mechanisms A–C above predict Scatchard-like kinetics relative to inhibitor concentrations under these conditions, this approach does not provide the information that allows us to assess which of these models might explain the fast-acting slow-binding paradigm.

The present studies are aimed at deriving kinetic equations that may best characterize inhibitor binding conforming to each of mechanisms A–C. The proposed theoretical approach takes on a quite general significance and involves models of arbitrary dimension on the rationale that realistic transport and enzyme mechanisms are usually more complex than the elementary reaction schemes used by Morrison and Walsh (1988) to describe the steady-state approach. Moreover, because the limitations associated with the steady-state formalism to assess inhibitor binding mechanisms apply to both transport processes (see Note 3) and enzyme reactions (Morrison and Walsh, 1988), the question of protein-inhibitor interactions is addressed with regard to the direct measurement of inhibitor binding to a protein. We therefore assume throughout this paper: 1) that an adequate assay has been found to measure, in a time-dependent way, the fraction of inhibitor bound to the relevant protein-inhibitor complexes, 2) that the progress of inhibitor binding can be satisfactorily described at the experimental level by a monoexponential function, and 3) that the binding data to be analyzed have been adequately corrected for nonspecific binding. Using this formalism, it is demonstrated that each of mechanisms A–C can be readily identified according to the position of the inhibitor binding step relative to the rate-limiting step in the inhibitor binding sequence. This key structural feature is the main determinant of unique kinetic properties that should allow anyone to determine unambiguously whether the inhibitor binding step either (A) represents, (B) precedes, or (C) follows the rate-limiting step. It is further shown that the relevance of mechanism C to slow-binding inhibition is conditioned by the turnover rate of the catalytic cycle under symmetrical conditions, and that mechanism B represents the only alternative to explain the fast-acting slow-binding paradigm of phlorizin.

MATERIALS AND METHODS

Time scale separation hypothesis and basic model

To reduce the complexity of the mathematics involved in deriving the characteristic equations for models of arbitrary dimension, it is appropriate to introduce approximations based on the principle that some reaction steps are faster than others, so that the time course of inhibitor binding to be observed will be governed by the slowest steps (Wierzbicki et al., 1990). In the following, we limit our analyses to the case where the progress of inhibitor binding can be satisfactorily described at the experimental level by a monoexponential function. This simplifying assumption allows us to compare our results with those of the steady-state approach pioneered by Morrison and Walsh (1988).

The kinetic mechanism shown in Fig. 1 *A* represents the simplest scheme that satisfies the above requirements, and the question of its relevance to more realistic kinetic mechanisms will be addressed in the Discussion. This model assumes that the binding of an arbitrary number of A_i effector molecules to a protein N can be described by a linear array of elementary reactions among which a slow isomerization (conformational change) with rate constants k_{on} and k_{off} represents the only rate-limiting

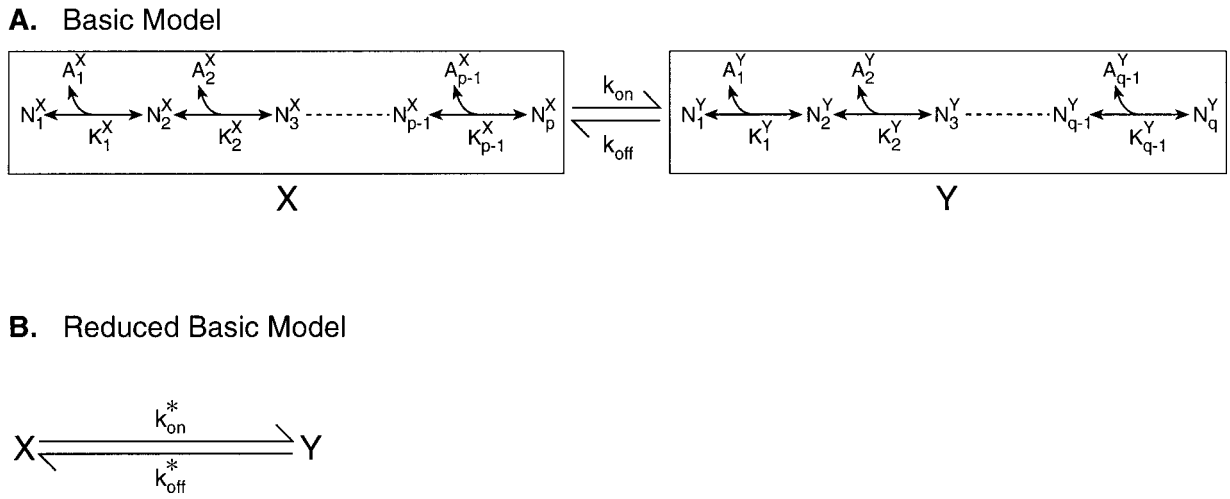

FIGURE 1 Basic model used for detailed kinetic analyses. (*A*) The structure of the basic model is composed of a linear array of elementary reactions, only one of which may be considered to be rate-limiting for the relaxation process with association and dissociation rate constants k_{on} and k_{off}, respectively. All the other reactions thus satisfy the rapid equilibrium assumption, which allows us to define the two blocks of elementary reactions X and Y. The N_i species may represent any protein under its free form (N_1) or following complexation with A_i effectors, each complex formation being described by a dissociation constant K_i. (*B*) Reduced basic model according to Cha's formalism (Cha, 1968) in which the apparent rate constants k^*_{on} and k^*_{off} defined in Eqs. 1 and 2 in the text now replace the true rate constants k_{on} and k_{off}.

step within the reaction sequence. This hypothesis is equivalent to stating that all the rate constants governing the association and dissociation of the A_i effectors with the protein are fast compared to k_{on} and k_{off}. Therefore, it is possible to define two blocks of elementary reactions called *X* and *Y*, in which all the chemical species can be considered to be in equilibrium with each other (rapid equilibrium assumption) both before and during the time-dependent slow interconversion between blocks *X* and *Y* (Cha, 1968; Wierzbicki et al., 1990). This, in turn, allows us to introduce the dissociation constants K_i^X and K_i^Y to describe each of the A_i binding steps within blocks *X* and *Y*, respectively. Note that the inhibitor binding step has not been included at this stage of the analysis to initially establish the most general solution describing the time-dependent interconversion (relaxation) between blocks *X* and *Y*, and to avoid redundancy in the derivation of more specific solutions applying to the different mechanisms of inhibitor binding, which will be considered later.

Time-dependent solution of the basic model

In the following, it is postulated that the concentrations of all of the A_i effectors present in the incubation media are constant over time and represent their total concentrations. For simplicity at this point, one may assume that none of the A_i effectors in the *X* and *Y* blocks is a substrate involved in a catalytic process, a hypothesis that will be relaxed in the Discussion.

According to Cha's rules (Cha, 1968), the general scheme depicted in Fig. 1 *A* can be reduced to its equivalent form shown in Fig. 1 *B* where the apparent rate constants k^*_{on} and k^*_{off} are defined as

$$k^*_{on} = k_{on} f_p^X, \tag{1}$$

$$k^*_{off} = k_{off} f_1^Y, \tag{2}$$

and now replace the true rate constants k_{on} and k_{off}. The latter are weighted by the factors f_p^X and f_1^Y, whose mathematical expressions,

$$f_p^X = \frac{N_p^X}{X} = \frac{N_p^X}{\sum_{i=1}^{p} N_i^X}, \tag{3}$$

$$f_1^Y = \frac{N_1^Y}{Y} = \frac{N_1^Y}{\sum_{i=1}^{q} N_i^Y}, \tag{4}$$

clearly indicate that they represent the fractional concentrations of the chemical species N_p^X and N_1^Y within blocks *X* and *Y*, respectively. The denominators of Eqs. 3 and 4 can be expressed relative to the N_p^X and N_1^Y species as

$$X = N_p^X(1 + L^X), \tag{5}$$

$$Y = N_1^Y(1 + L^Y), \tag{6}$$

where algebraic expressions of the quantities L^X and L^Y

$$L^X = \sum_{i=1}^{p-1} \prod_{j=i}^{p-1} \frac{K_j^X}{A_j^X}, \tag{7}$$

$$L^Y = \sum_{i=1}^{q-1} \prod_{j=1}^{i} \frac{A_j^Y}{K_j^Y}, \tag{8}$$

are conditioned by the rapid equilibrium assumption. Note that the two blocks, *X* and *Y*, are also linked through the conservation equation,

$$N_T = X + Y. \tag{9}$$

The time-dependent interconversion between blocks *X* and *Y* can be described by the differential equation

$$\frac{dY}{dt} = -\frac{dX}{dt} = k_{on} N_p^X - k_{off} N_1^Y = k^*_{on} X - k^*_{off} Y, \tag{10}$$

in which the right-hand-side expression results from the consideration of Eqs. 3–6 and can be transformed as

$$\frac{dY}{dt} = k^*_{on} N_T - (k^*_{on} + k^*_{off})Y, \quad (11)$$

by incorporating Eq. 9. Equation 11 can be further rearranged as

$$\frac{dY}{dt} + k_{obs}Y = k_{obs}Y_e, \quad (12)$$

with the definitions for k_{obs} (apparent first-order rate of the relaxation process)

$$k_{obs} = k^*_{on} + k^*_{off}, \quad (13)$$

and Y_e (equilibrium concentration of Y at the end of the relaxation process),

$$Y_e = \frac{k^*_{on} N_T}{k_{obs}}. \quad (14)$$

The integration of Eq. 12 over time is straightforward and leads to equivalent monoexponential functions

$$\begin{aligned} Y &= Y_e - (Y_e - Y_0)e^{-k_{obs}t} \\ &= Y_0 + (Y_e - Y_0)(1 - e^{-k_{obs}t}), \end{aligned} \quad (15)$$

in which Y_0 represents the zero-time concentration of Y at the start of the relaxation. Note that the evaluation of Y_0 shall depend on the specific kinetic mechanisms to be considered later. A last quantity that may be measured experimentally is the initial rate of interconversion (Y_i), the mathematical expression of which can be readily obtained from the first derivative of Eq. 15 at $t = 0$, as

$$Y_i = \left[\frac{dY}{dt}\right]_{t=0} = k_{obs}(Y_e - Y_0). \quad (16)$$

Note that Eq. 10 could have been made homogeneous relative to X to describe the same phenomenon with the differential equation

$$\frac{dX}{dt} = k^*_{off} N_T - (k^*_{on} + k^*_{off})X \quad (17)$$

as a result, the integration of which leads to

$$X = X_0 + (X_e - X_0)(1 - e^{-k_{obs}t}), \quad (18)$$

where the quantity X_0 (zero-time concentration of X) should reflect the boundary conditions applying to each specific mechanism while X_e (equilibrium concentration of X) represents the solution of Eq. 17 when $dX/dt = 0$,

$$X_e = \frac{k^*_{off} N_T}{k_{obs}} = \frac{k^*_{off} Y_e}{k^*_{on}}. \quad (19)$$

Inhibitor-binding mechanisms and further assumptions

If inhibitor binding is now considered in the kinetic schemes shown in Fig. 1, it is readily apparent that only three possibilities may be viewed whereby the inhibitor binding step either represents (mechanism A), precedes (mechanism B) or follows (mechanism C) the rate-limiting step. As depicted in Fig. 2, these three mechanisms are associated with the assumptions 1) there is only one inhibitor binding site, so that inhibitor binding at equilibrium should conform to Scatchard kinetics relative to the free concentration of inhibitor [I], 2) the inhibitor binding site is accessible through only one of the N_i species, and 3) the total concentration of inhibitor (I_T) far exceeds the total concentration of binding sites (N_T), so that $[I] \approx I_T$ and [I] can be considered constant during the time interval over which the binding assay is performed. Note that the relaxation of assumptions 1 and 2 will be considered in the Discussion whereas assumption 3 excludes from consideration the so-called tight-binding inhibitors for which there is not a single rate equation for the time course, but rather a pair of parametric equations that describe the progress curves at different inhibitor concentrations (Sculley et al., 1996). Also, with the current hypothesis that none of the A_i effectors is a substrate involved in a catalytic process, mechanisms A–C in Fig. 2 are quite general and may describe the kinetics of inhibitor (or any other molecule) binding to any protein independent of the time scale of the observation, which is conditioned by the nature of the binding assay and limited by the absolute values of k^*_{on} and k^*_{off}. The question of the applicability of mechanisms A–C to fast-acting and slow-binding inhibitions is addressed in the Discussion.

The formalism previously discussed and justified by Wierzbicki et al. (1990) for presteady-state kinetics can now be used to identify time-dependent solutions of inhibitor binding provided that the following assumptions, with regard to the conditions of the binding assays, are introduced. We first assume that the relevant preparations to be tested for inhibitor binding have been sufficiently resuspended in the uptake media to ensure that true equilibrium conditions have been reached with each of the A_i effector molecules at the time of the assay, so that it is possible to calculate the boundary conditions (X_{00} and Y_{00}) prevailing before the start of the binding assay. We next assume that the binding assay is started by mixing the above preparations in identical media containing the inhibitor to be tested, so that there will be fast redistribution only of those N_i^X or N_i^Y species involved in rapid equilibrium reactions with the inhibitor. Accordingly, it is possible to calculate the boundary conditions (X_0 and Y_0) prevailing at the very start of the relaxation process when $t = 0$. Finally, because, in mechanisms B and C, the rates of association and dissociation of the inhibitor are fast compared to k^*_{on} and k^*_{off}, one may also need to consider that some binding assays, including the rapid filtration technique, may fail to detect most (if not all) of the inhibitor molecules bound to the N_i^X or N_i^Y species in each of these models, respectively.

To avoid redundancy in the writing of both similar equations and the definitions of similar parameters, reference is made throughout the text to the Scatchard or Michaelis–Menten equation

$$B = \frac{B_{max}(I)}{K_d + (I)}, \quad (20)$$

in which B represents the amount of inhibitor molecules bound to its specific site on the protein, (I) stands for the free concentration of inhibitor (but $I \approx I_T$, see above)), and B_{max} (apparent maximum number of binding sites) and K_d (apparent dissociation constant for inhibitor binding) are the usual kinetic parameters of interest to be determined. The indices 0, i, and e associated with these parameters consistently represent the kinetic situation that prevails, respectively, at the very start of the binding assay when $t = 0$, over the time period during which it can be assumed that true initial rates of binding can be measured, and at equilibrium when a steady-state plateau value has been reached. When necessary, the kinetic parameter

$$K_{XY} = \frac{k_{off}}{k_{on}} \quad (21)$$

is introduced, which represents the dissociation constant characterizing the rate limiting step. Note that $K_{XY} = K_d$ (intrinsic dissociation constant for inhibitor binding) in mechanism A only.

All calculations involving complex algebraic expressions have been performed using Mathematica software for Windows. For the more specific cases discussed in the Appendix, the initial velocity equations and the relevant distribution equations are derived using computer calculations described elsewhere (Falk et al., 1998).

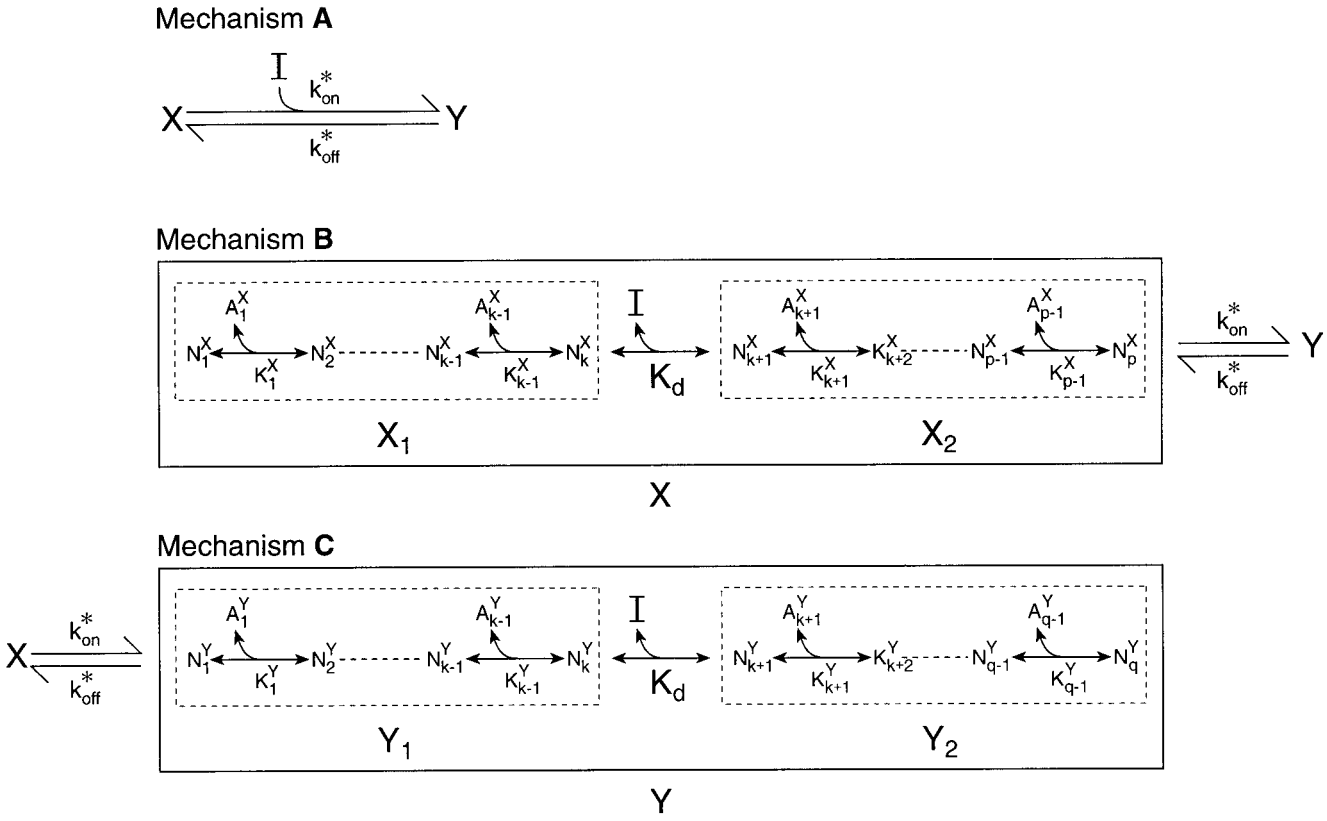

FIGURE 2 The three kinetic mechanisms that may account for slow inhibitor binding. (*A*) Extension to a dimensionless model of previous mechanism A (Morrison and Walsh, 1988), in which inhibitor binding may itself represent the rate-limiting step. (*B*) Extension to a dimensionless model of previous mechanism B (Morrison and Walsh, 1988), in which fast inhibitor binding with dissociation constant K_d is followed by a slow isomerization step. Before inhibitor addition, all the N_i species are constrained within subblock X_1, so that $X_{00} = X_1 = N_T$. Once added, the inhibitor promotes fast redistribution of the N_i^{X1} species between subblocks X_1 and X_2, forming the new X block, so that $X_0 = N_T$. The relaxation process between blocks X and Y follows thereafter. (*C*) Application to a dimensionless model of the recruitment hypothesis (Aronson, 1978; Turner and Silverman, 1980), in which a slow conformational change controls the rate of inhibitor binding with dissociation constant K_d. Before inhibitor binding, there is a true equilibrium between block X and subblock Y_1. Once added, the inhibitor promotes fast redistribution of the N_i^{Y1} species between subblocks Y_1 and Y_2, forming the new Y block, and the relaxation process between blocks X and Y follows thereafter. When not given in details in mechanisms A–C, the structure of the elementary reactions occurring in blocks X and Y is identical to that shown in Fig. 1 *A*. The apparent rate constants k^*_{on} and k^*_{off} are defined by Eqs. 1 and 2 in the text except for mechanism A, in which Eq. 22 should be substituted for Eq. 1.

RESULTS

Mechanism A: Inhibitor binding is the rate-limiting step

To solve mechanism A, the basic model depicted in Fig. 1 *A* only needs to be modified to include inhibitor binding to the N_p^X species as shown, under reduced form, in Fig. 2 *A*. Accordingly, Eqs. 2–9 still apply to this model while a correct expression for k^*_{on} should now read as follows.

$$k^*_{on} = k_{on} f_p^X(I). \tag{22}$$

Moreover, because all the N_i species in block *Y* contribute to the binding equation, the time course of inhibitor binding will be described by Eq. 15 in which *B* is substituted for *Y*, and k_{obs} is given by Eq. 13. The boundary conditions

$$X_{00} = X_0 = N_T; \quad Y_{00} = Y_0 = B_0 = 0 \tag{23}$$

are easily established from our assumptions regarding the binding assay conditions (see the section entitled "Inhibitor-binding mechanisms and further assumptions" under Materials and Methods). The quantities $B_e = Y_e$ and $B_i = Y_i$ can also be found from proper substitution into Eq. 14 and 16, respectively. A few arithmetic manipulations using the relevant equations above are necessary to derive the algebraic expressions of the different kinetic parameters shown in Tables 1 and 2.

Mechanism B: Binding of the inhibitor precedes the rate-limiting step

General considerations

The analysis of mechanism B requires an expansion of the basic model depicted in Fig. 1 *A* to include an inhibitor binding step within the *X* block. The resulting reduced scheme is shown in Fig. 2 *B*, from which the boundary conditions appear similar to those previously established for mechanism A (Eq. 23). Eqs. 2, 4, 6, and 8, which all apply

TABLE 1 Kinetic characteristics of the three mechanisms of inhibitor binding depicted in Fig. 2

Experimental Parameters	Kinetic Mechanisms			
	A	B occluded	B general	C
B_0	0	0	$\frac{B_{max0}(I)}{K_{d0}+(I)}$	$\frac{B_{max0}(I)}{K_{d0}+(I)}$
B_i	$\frac{k_{on}N_T(I)}{1+L^X}$	$\frac{B_{maxi}(I)}{K_{di}+(I)}$	$\frac{B_{maxi}K_{di}(I)}{[K_{di}+(I)]^2}$	$\frac{B_{maxi}(I)^2}{[K_{di}+(I)]^2}$
B_e	$\frac{B_{maxe}(I)}{K_{de}+(I)}$	$\frac{B_{maxe}(I)}{K_{de}+(I)}$		$\frac{B_{maxe}(I)}{K_{de}+(I)}$
k^*_{on}	$\frac{k_{on}(I)}{1+L^X}$	$\frac{k_{on}(I)}{\beta K_d(1+L_1^X)+(1+L_2^X)(I)}$		$\frac{k_{on}}{1+L^X}$
k^*_{off}	$\frac{k_{off}}{1+L^Y}$	$\frac{k_{off}}{1+L^Y}$		$\frac{k_{off}K_d}{K_d(1+L_1^Y)+\alpha(I)(1+L_2^Y)}$
k_{obs}	linear increase	hyperbolic increase		hyperbolic decrease

The experimental parameters are defined relative to a family of progress curves generated at different concentrations of the inhibitor as follows: B_0, zero-time intercept; B_i, initial rate of binding; B_e, equilibrium binding; k^*_{on} and k^*_{off}, apparent first-order rates of inhibitor association to and dissociation from the protein; k_{obs}, apparent first-order rate of the relaxation process as given by Eq. 13. B_{max0}, B_{maxi}, B_{maxe}, K_{d0}, K_{di}, and K_{de} represent the usual kinetic parameters of interest to be determined, and their algebraic expressions are reported in Table 2. All the other constants are defined in the text.

to the Y block, are still valid as shown in this particular case, hence the algebraic expression of k^*_{off} shown in Table 1. Similarly, Eqs. 1 and 3 referring to block X still hold; however, Eq. 5 needs to be rewritten as

$$X = N_p^X\left[1 + L_2^X + \beta\frac{K_d}{(I)}(1+L_1^X)\right], \tag{24}$$

to account for the inhibitor binding step. The algebraic expression of k^*_{on} appearing in Table 1 follows from these considerations whereas those of the new parameters appearing in Eq. 24 are as

$$L_2^X = \sum_{i=k+1}^{p-1}\prod_{j=i}^{p-1}\frac{K_j^X}{A_j^X}, \tag{25}$$

$$\beta = \prod_{j=k+1}^{p-1}\frac{K_j^X}{A_j^X}, \tag{26}$$

$$L_1^X = \sum_{i=1}^{k-1}\prod_{j=i}^{k-1}\frac{K_j^X}{A_j^X}. \tag{27}$$

At this stage in the analysis of mechanism B, it is important to question to what extent the inhibitor-bound $N_i^X(B^X = X_2)$ and $N_i^Y(B^Y = Y)$ species contribute to the binding equation, $B = B^X + B^Y$, in actual experiments. Indeed, most (if not all) of the inhibitor molecules bound to the N_i^X species might be lost in any binding assay involving a

TABLE 2 Algebraic expressions of the kinetic parameters appearing in the equations reported in Table 1

Kinetic Parameters	Kinetic Mechanisms			
	A	B occluded	B general	C
B_{max}	0	0	N_T	$\frac{(1+L_1^Y)N_T}{1+L_1^Y+K_{XY}(1+L^X)}$
K_{d0}	0	0	$\frac{\beta(1+L_1^X)K_d}{1+L_2^X}$	$\frac{(1+L_1^Y)K_d}{\alpha(1+L_2^Y)}$
B_{maxi}	—	$\frac{k_{on}N_T}{1+L_2^X}$		$\frac{k_{on}K_{XY}N_T}{1+L_1^Y+K_{XY}(1+L^X)}$
K_{di}	—	$\frac{\beta(1+L_1^X)K_d}{1+L_2^X} = K_{d0}$		$\frac{(1+L_1^Y)K_d}{\alpha(1+L_2^Y)} = K_{d0}$
B_{maxe}	N_T	$\frac{(1+L^Y)N_T}{1+L^Y+K_{XY}(1+L_2^X)}$	N_T	N_T
K_{de}	$\frac{(1+L^X)K_d}{1+L^Y}$	$\frac{\beta K_{XY}(1+L_1^X)K_d}{1+L^Y+K_{XY}(1+L_2^X)}$		$\frac{[1+L_1^Y+K_{XY}(1+L^X)]K_d}{\alpha(1+L_2^Y)}$

All the constants appearing in the algebraic expressions shown are defined in the text.

quench technique to stop the reaction, because the time scale separation hypothesis clearly states that all the dissociation rates associated with the inhibitor-bound N_i^X species are fast as compared to k_{off}^* (see also the sections entitled "Time scale separation hypothesis and basic model" and "Inhibitor-binding mechanisms and further assumptions" under Materials and Methods). In contrast, as in mechanism A, the inhibitor bound N_i^Y species would appear as occluded under these conditions in that the inhibitor molecules bound to these species are shielded by the rate-limiting step from free exchange with the external milieu.

The binding equation involves the N_i^Y species only: The occlusion case

From the above description, it is readily apparent that a situation in which $B^X = 0$ can be favored in a radiotracer assay, either voluntarily or not, by including a saturating concentration of the unlabeled inhibitor (or a competitive substrate or effector) in the quench solution. In this case, the time course of inhibitor binding will be described by Eq. 15, in which B^Y is substituted for Y, k_{obs} is given by Eq. 13, and $B_0^Y = 0$ (Eq. 23). Similarly, the quantities $B_e^Y = Y_e$ and $B_i^Y = Y_i$ can be obtained from proper substitution into Eq. 14 and 16, respectively. A few arithmetic manipulations using the relevant equations above are necessary to get the algebraic expressions of the different kinetic parameters shown in Tables 1 and 2. It can be further demonstrated that the relationship

$$\frac{K_{de}}{K_{di}} \cdot \frac{B_{maxi}^Y}{B_{maxe}^Y} = \frac{k_{off}}{1 + L^Y} = k_{off}^* \tag{28}$$

applies, thus providing an internal consistency test of the model.

The binding equation involves both the N_i^X and N_i^Y species: The general case

If all of the inhibitor-bound species can be detected in the assay, then the binding function should also include the B^X term, which can be expressed relative to N_p^X, as

$$B^X = X_2 = \sum_{i=k+1}^{p} N_i^X = (1 + L_2^X)N_p^X, \tag{29}$$

when accounting for the rapid equilibrium assumption. It is thus possible to calculate the fractional concentration of the chemical species to which the inhibitor is bound in the X block (f_b^X) by combining Eqs. 24 and 29 as

$$f_b^X = \frac{B^X}{X} = \frac{(1 + L_2^X)(I)}{\beta K_d(1 + L_1^X) + (1 + L_2^X)(I)}. \tag{30}$$

Because the latter equation holds true at both $t = 0$ and at equilibrium (see the section "Inhibitor-binding mechanisms and further assumptions" under Materials and Methods), the time-dependent relaxation of B^X will be described by the quantity $f_b^X X$, in which X is given by Eq. 18. The quantity $B_e^X = f_b^X X_e$ (number of binding sites in block X at equilibrium) can be computed from Eq. 19 and rearranged under the Scatchard form,

$$B_e^X = \frac{B_{maxe}^X(I)}{K_{de} + (I)}$$

where

$$B_{maxe}^X = \frac{K_{XY}(1 + L_2^X)N_T}{1 + L^Y + K_{XY}(1 + L_2^X)} \leq N_T, \tag{31}$$

in which the algebraic expression of K_{de} is identical to that previously established in the occluded case (Table 2). Similarly, the quantity $B_0 = f_b^X X_0$ (initial binding at $t = 0$) can be found using the boundary conditions given by Eq. 23 and cast under the Scatchard form shown in Table 1, with algebraic expressions of the kinetic parameters as reported in Table 2. Note that K_{d0} in the general case is equal to K_{di} in the occluded case, and that the quantity

$$B_e^X - B_o = -\frac{(1 + L^Y)N_T(I)^2}{[1 + L^Y + K_{XY}(1 + L_2^X)][K_{di} + (I)][K_{de} + (I)]} \tag{32}$$

has a negative sign, indicating that the number of inhibitor molecules bound to the block X species decreases with time.

It is now possible to derive the time-dependent equation that describes the kinetics of inhibitor binding B by summing up the two exponential functions B^X and B^Y. The final result is similar in form to Eq. 15, but where B is substituted for Y, with B_0 already given in Tables 1 and 2 and the quantity $B_e = B_e^X + B_e^Y$ calculated from Table 2 and Eq. 31. Note that B_e is the sum of two Scatchard equations with identical denominators, so that the relationship $B_{maxe} = B_{maxe}^X + B_{maxe}^Y = N_T$ can be readily established. Similarly, a correct expression of B_i can be computed from Eq. 16 with proper substitutions therein, and a few arithmetic calculations show that B_i can be cast under the generic form shown in Table 1 with algebraic expressions of B_{maxi} and K_{di} as given in Table 2. Accordingly, at increasing concentrations of the inhibitor, the initial rate data should first increase to reach a maximum value equivalent to $B_{maxi}/4$ when $(I) = K_{di}$ and decrease toward zero thereafter.

Mechanism C: Binding of the inhibitor follows the rate-limiting step

To solve this kinetic mechanism, the basic scheme depicted in Fig. 1 *A* also needs to be expanded to include an inhibitor-binding step within the Y block as shown in Fig. 2 *C*. Note that the Y_2 block, which represents the fraction of inhibitor molecules bound to the N_i^Y species, is not protected from free exchange with the external milieu in this particular case. Therefore, inhibitor binding may not be measurable using a radiotracer technique in combination with a

rapid filtration assay. Subject to this experimental limitation, the following theoretical considerations are nevertheless right.

Eqs. 1, 3, 5, and 7, which all apply to the X block, are still valid as shown in this case, hence the algebraic expression of k^*_{on} appearing in Table 1. Similarly, Eqs. 2 and 4, referring to the Y block, still hold; however, Eq. 6 needs to be rewritten as

$$Y = N_1^Y\left[1 + L_1^Y + \alpha\frac{(I)}{K_d}(1 + L_2^Y)\right] \tag{33}$$

to account for the inhibitor binding step. The algebraic expression of k^*_{off} appearing in Table 1 follows from these considerations, whereas those of the new parameters appearing in Eq. 33 are given as

$$L_1^Y = \sum_{i=1}^{k-1}\prod_{j=1}^{i}\frac{A_j^Y}{K_j^Y}, \tag{34}$$

$$\alpha = \prod_{j=1}^{k-1}\frac{A_j^Y}{K_j^Y}, \tag{35}$$

$$L_2^Y = \sum_{i=k+1}^{q-1}\prod_{j=k+1}^{i}\frac{A_j^Y}{K_j^Y}. \tag{36}$$

In this model, the binding function,

$$B = Y_2 = \sum_{i=k+1}^{q} N_i^Y = \alpha\frac{(I)}{K_d}(1 + L_2^Y)N_1^Y, \tag{37}$$

and the fractional concentration of the chemical species to which the inhibitor is bound in the Y block,

$$f_b^Y = \frac{B}{Y} = \frac{\alpha(I)(1 + L_2^Y)}{K_d(1 + L_1^Y) + \alpha(I)(1 + L_2^Y)}, \tag{38}$$

can be readily written from a visual inspection of Fig. 2 *C*. Because the latter relationships hold true at both $t = 0$ (when $B_0 = f_b^Y Y_0$) and equilibrium (when $B_e = f_b^Y Y_e$), the time course of inhibitor binding should thus be described by Eq. 15, in which B is substituted for Y, k_{obs} is given by Eq. 13, and the quantity B_e found from proper substitution into Eq. 14. A few arithmetic manipulations are necessary to get the algebraic expressions of the kinetic parameters shown in Table 2. A correct expression of B_i can be derived from Eq. 16 as

$$B_i = k_{obs}f_b^Y(Y_e - Y_o) = k_{obs}(B_e - B_o). \tag{39}$$

One thus needs to define the boundary conditions to determine the algebraic expression of the initial rate of binding. This is done as follows. Because there is a true equilibrium between the block X ($= X_{00}$) and the subblock Y_1 ($= Y_{00}$) before addition of the inhibitor (see the section "Inhibitor-binding mechanisms and further assumptions" under Materials and Methods), it is possible to write down the set of equations,

$$X_{00} + Y_{00} = N_T, \tag{40}$$

$$k^*_{on}X_{00} = k^*_{off}Y_{00}. \tag{41}$$

When solved in conjunction with Eqs. 1–5 and 33 (in which $[I] = 0$ before the start of the experiment), the algebraic expression,

$$Y_{00} = \frac{N_T(1 + L_1^Y)}{1 + L_1^Y + K_{XY}(1 + L^X)}, \tag{42}$$

can be obtained following a few arithmetic manipulations. Because $Y_0 = Y_{00}$ in this particular case (see the section "Inhibitor-binding mechanisms and further assumptions" under Materials and Methods), then $B_o = f_b^Y Y_{00}$ with f_b^Y and Y_{00} as given by Eqs. 38 and 42, respectively. B_0 can be cast under the Scatchard form given in Table 1 with algebraic expressions of the kinetic parameters as reported in Table 2. The initial rate of binding can now be calculated from Eq. 39 and proper substitutions therein. B_i can be cast under the generic form shown in Table 1 with algebraic expressions of B_{maxi} and K_{di} as given in Table 2. The B_i versus $[I]$ plot should clearly deviate from simple Scatchard kinetics, and the apparent Hill number value (n_H) that one may expect from a Hill plot analysis of the initial rate data can be estimated from the relationship

$$n_H = \left[\frac{d\,Ln[B_i/(B_{maxi} - B_i)]}{d\,Ln(I)}\right]_{(I)_{0.5}} = \left[\frac{B_{maxi}(I)}{B_i(B_{maxi} - B_i)}\cdot\frac{dB_i}{d(I)}\right]_{(I)_{0.5}}, \tag{43}$$

which was previously derived from a similar equation (Falk et al., 1998). The $(I)_{0.5}$ expression,

$$(I)_{0.5} = K_{do}(1 + \sqrt{2}), \tag{44}$$

can be found by solving the B_i equation in Table 1 for (I) after setting $B_i = B_{maxi}/2$, whereas the formal development of the terms in brackets at the right-hand-side of Eq. 43 leads to

$$n_H = 1 + \frac{K_{do}}{K_{do} + 2(I)_{0.5}}, \tag{45}$$

and then to $n_H = 1.17$ when Eqs. 44 and 45 are combined. Accordingly, the sigmoidicity predicted in the B_i versus $[I]$ plot may not be easily detected at the experimental level, particularly because the inflexion point occurs in the very early part of the curve when $(I) = K_{do}/2$.

DISCUSSION

Kinetic criteria aimed at model discrimination

The results presented in these studies clearly demonstrate that the three basic mechanisms of inhibitor binding de-

picted in Fig. 2 are associated with a set of kinetic features which could be easily investigated at the experimental level by the analysis of a family of binding time courses generated at different concentrations of the inhibitor as follows

1. As shown in Table 1, all curves should either go through the origin [mechanisms A and B (occluded)] or intercept the y axis at discrete B_0 values [mechanisms B (general) and C]. In the latter situation, a B_0 versus (I) plot should demonstrate Scatchard kinetics from which either the total [mechanisms B (general)] or apparent (mechanism C) number of binding sites, and the initial apparent dissociation constant for inhibitor binding (K_{d0}) can be determined (Table 2).
2. The initial rate of binding (B_i in Table 1) should saturate at increasing inhibitor concentrations in mechanisms B (occluded) and C. For the latter, the binding data deviates from simple Scatchard kinetics (note that it might prove difficult to detect the sigmoidicity of the B_i versus [I] plot at the experimental level, see Eqs. 43–45), and the K_{di} value estimated from its kinetic analysis should be identical to the K_{d0} value. In contrast, B_i should increase linearly with [I] in mechanism A, and so, the initial rate data might be mistakenly thought to represent nonspecific binding. In mechanism B (general) too, the B_i versus [I] plot deviates from simple Scatchard kinetics and the data curve first increases to a maximum value and then decreases toward 0.
3. When the inhibitor binding step either precedes (mechanism B) or itself represents (mechanism A) the rate-limiting step, the k^*_{on} value only, and not the k^*_{off}, is affected by [I], whereas the reverse situation holds true in mechanism C, where the inhibitor binds downstream of the rate-limiting step (Table 1). Consequently, according to Eq. 13, k_{obs} should linearly increase and hyperbolically decrease in mechanisms A and C, respectively. In contrast, mechanism B predicts a Scatchard-like dependence of the k_{obs} versus [I] plot with an intercept value on the y axis representing the apparent first-order rate for dissociation of the inhibitor. Note that the algebraic expression of k^*_{on} in Table 1 can be further rearranged as

$$k^*_{on} = \frac{k^{max}_{on}(I)}{K_{di} + (I)}, \tag{46}$$

where

$$k^{max}_{on} = \frac{k_{on}}{1 + L_2^X} = \frac{B_{maxi}}{N_T}, \tag{47}$$

to demonstrate that the half-saturation of k_{obs} is achieved when [I] = K_{di} (occluded case) = K_{d0} (general case), thus providing an internal test of mechanism B. A similar rearrangement of the algebraic expression of k^*_{off} for mechanism C in Table 1 could be performed to show that the value of this parameter is reduced by half at [I] = K_{d0}.
4. As expected from the assumption that there is only one inhibitor binding site, the B_e versus [I] plot should saturate for all mechanisms, and a Scatchard analysis of the equilibrium data should allow one to determine the apparent dissociation constant of the inhibitor and the total number of binding sites except for mechanism B (occluded) in which $B_{maxe} < N_T$ (Table 2). In the latter case, N_T can only be calculated, and this is easily done using Eq. 47. A comparison of the algebraic expressions of K_{de} and of either K_{di} or K_{d0}, shown in Table 2 for mechanism B, allows us to establish,

$$\frac{K_{de}}{K_{di}} = \frac{K_{XY}(1 + L_2^X)}{1 + L^Y + K_{XY}(1 + L_2^X)} \leq 1, \tag{48}$$

that the apparent affinity for inhibitor binding estimated at equilibrium should always be higher than that observed during the initial phase of binding. In contrast, the relationship

$$\frac{K_{de}}{K_{do}} = 1 + K_{XY}\frac{1 + L^X}{1 + L_1^Y} \geq 1 \tag{49}$$

is always predicted in the case of mechanism C. It can be concluded that the value of the K_{de}/K_{di} ratio is determined by kinetic properties that appear intrinsic to mechanisms B and C, so that this parameter takes on particular relevance for model discrimination.

Among these kinetic features, the dependence on inhibitor concentration of the apparent first-order rate of binding k_{obs} appears to be the most reliable indicator for diagnostic purposes. Its analysis should thus allow one to establish unambiguously whether the inhibitor binding step itself or a step that either precedes or follows inhibitor binding represents the overall rate-limiting step in a binding process. However, this conclusion raises the question of the predictive value of the basic schemes shown in Figs. 1 and 2 when applied to more complex models and to transport mechanisms in particular.

Validity of the predictions of the basic scheme with regard to more complex models and transport mechanisms

It could be argued that the simplistic nature of the basic models depicted in Figs. 1 and 2 may restrict the validity of our studies to just a few realistic kinetic mechanisms. This argument is refuted below, where it clearly appears that our results are, in fact, conditioned by the structure of the reduced kinetic scheme shown in Fig. 1 *B*.

Equations similar in form to Eqs. 5 and 6 can be derived for any kinetic mechanism to which the rapid equilibrium assumption applies. This assertion follows from Cha's rule, stating that, when there is more than one pathway through which N_i may be converted to N_j in a rapid equilibrium segment, any one and only one of these pathways may be used for the evaluation of N_j relative to N_i (Cha, 1968).

Accordingly, either one or both of the *X* and *Y* blocks shown in Fig. 1 *B* could include any number of cycles, random sequences of effector addition, and/or branched pathways. In addition, the rate-limiting step linking these two blocks could involve any of the N_i^X and/or N_i^Y species. In such cases, the algebraic expressions of L^X and L^Y might be more complex than those shown in Eqs. 7 and 8 and include both K_j/A_j and A_j/K_j terms for those effector molecules which, respectively, dissociate from or associate with the N_i^X and/or N_i^Y species linking the two blocks. Accordingly, it can be predicted that low upstream or high downstream effector concentrations relative to location of N_i^X would both act to decrease the apparent value of k_{obs} (increase the time constant of the relaxation process). Such a situation has been described for the slow binding of ^{3}H-ouabain to Na^+,K^+-ATPase, which was found to be accelerated by Na^+ and retarded by K^+, thus suggesting that Na^+ and K^+ modulate glycoside interaction through an induction (Na^+) or repression (K^+) of the macromolecular conformation appropriate for glycoside binding (Schwartz et al., 1974). In this particular case, the inhibitor binding step itself represents the rate-limiting step of the ouabain binding process, a conclusion that was reached on the ground that k_{obs} increases linearly with glycoside concentrations, in agreement with the results of our studies using the basic model shown in Fig. 2 *A*.

More complex situations could arise if rate-limiting steps exist within cycles as may occur in transport mechanisms (see examples given in the Appendix) and other kinetic mechanisms showing random sequences of effector and/or inhibitor addition. In such cases, the predictive value of the basic models depicted in Fig. 2 will not be affected provided that:

1. the rate-limiting steps isolate two clearly identifiable blocks. This condition is essential for applying the rule of additivity of parallel pathways proposed by Volkenstein and Goldstein (1966), which would allow one to reduce the kinetic mechanism to a scheme similar in form to that shown in Fig. 1 *B*. Because this rule is not restrictive as to the number of rate-limiting steps connecting the two blocks, the expressions,

$$k^*_{on} = \sum_{i=1}^{n}(k^*_{on})_i = \sum_{i=1}^{n}(k_{on})_i f_i^X, \tag{50}$$

$$k^*_{off} = \sum_{i=1}^{n}(k^*_{off})_i = \sum_{i=1}^{n}(k_{off})_i f_i^Y, \tag{51}$$

   in which *n* represents the number of rate-limiting steps with rate constants $(k_{on})_i$ and $(k_{off})_i$, only need to be substituted for Eqs. 1 and 2, respectively. Note that all the f_i^X or f_i^Y fractions characterizing the N_i species involved in the relaxation process have identical denominators (Cha, 1968), so that their summation does not introduce $[I]^2$ terms.

2. all rate-limiting steps involve inhibitor binding, in which case the kinetic mechanism can be reduced to a scheme similar in form to that shown for mechanism A in Fig. 2, where the k^*_{on} expression,

$$k^*_{on} = \sum_{i=1}^{n}(k_{on})_i f_i^X(I) = (I)\sum_{i=1}^{n}(k_{on})_i f_i^X, \tag{52}$$

   only needs to be substituted for Eq. 22. Alternatively, the inhibitor molecule may bind either upstream or downstream of the rate-limiting steps, in which case the corresponding kinetic mechanisms can be reduced to schemes similar in form to those shown for mechanisms B and C in Fig. 2, respectively. Clearly, then, all of these situations would preserve the predictive value of k_{obs} for discrimination between mechanisms A and C (Table 1).

Note that the failure to satisfy condition 1 should result in binding time courses showing more than one relaxation constant; however, the B_e versus $[I]$ plot should still conform to Scatchard kinetics if only one inhibitor binding site is involved. Also, the failure to satisfy condition 2 should lead to a situation where the k_{obs} versus $[I]$ plot is more complex than predicted in spite of both monoexponential binding kinetics and of B_e versus $[I]$ plots conforming to Scatchard kinetics.

Finally, Cha's rule and the additivity principle above may be combined (Cha, 1968) to reduce almost any kinetic mechanism to the basic structure shown in Fig. 1 *B* provided that our hypotheses (see Materials and Methods) and the restrictions discussed above are respected. Thus, equations similar in form to Eqs. 24 and 33 may be derived for kinetic mechanisms in which the inhibitor binds to more than one of the N_i species involved in blocks *X* or *Y*. Because our analysis was restricted to the case of one inhibitor binding site only, this would preclude $[I]^2$ terms in the above equations under rapid equilibrium conditions. However, should there be more than one binding site in block *X* or *Y*, the predictive value of k_{obs} would be preserved: this parameter should still decrease or increase with the concentration of inhibitor in models B or C, respectively. Such mechanisms may then be recognized from the non-Scatchard dependence of the B_e versus $[I]$ plot.

Relevance of mechanisms A–C to fast-acting (classical) inhibitors and monoexponential kinetics

As noted earlier, fast-acting or slow-binding inhibition is not the result of mechanistic considerations but rests on the assumption that the two classes of inhibitors can be identified through the application of steady-state kinetic methods, i.e., on the time scale of seconds to minutes. However, our hypothesis that the kinetics of inhibitor binding can be described by monoexponential functions at the experimental level does not set any limit on the time scale over which this observation is made because the scale is dictated by the

absolute values of k^*_{on} and k^*_{off}. Therefore, mechanisms A–C in Fig. 2 could all apply to fast-acting inhibitors provided that the binding assay can resolve the kinetics of inhibitor binding on the presteady-state time scale. Over this subsecond time range, the condition that none of the A_i effectors is a substrate or product involved in a catalytic process could even be relaxed, so that these three mechanisms could also be used to analyze the presteady-state kinetics of transport processes or enzyme reactions according to the simplified approach proposed by our group (see Note 5) (Wierzbicki et al., 1990). For example, as was justified for a four-state model of carrier-mediated transport, two rate-limiting steps need to be considered to allow for monoexponential kinetics, and six submodels would satisfy this condition. Accordingly, the formalism described in the present paper may also be used to reduce all of these submodels to the general scheme shown in Fig. 1 *B*, so that the algebraic expression of the apparent first-order rate characterizing the relaxation process in each can now be readily obtained from the consideration of Eqs. 13 and 50–52. Indeed, this new approach leads to results that are identical to those reported by Wierzbicki et al. (1990) in his Table 4 (see Note 6). Moreover, as predicted in Table 1, k_{obs} assumes either a Michaelis–Menten or a linear dependence on substrate concentrations for those submodels in which, respectively, the rapid equilibrium addition of substrate induces the relaxation process (models 1, 2, and 4) or the substrate addition step itself represents the rate-limiting step (models 3, 5, and 6).

Relevance of mechanisms A and B to slow-binding inhibitors

The parallelism between mechanisms A and B shown in Fig. 2 and their elementary counterparts, previously described within the framework of steady-state enzyme kinetics (Morrison and Walsh, 1988), is straightforward if one assumes that enzyme-catalyzed reactions may only occur in block X and subblock X_1, respectively. However, because the concentration of all of the A_i effectors must also be constant with time as postulated under Materials and Methods, this hypothesis requires that the products be formed from N_i^X species (none of the A_i may be reaction products) and that the rate of product formation be faster than k^*_{on} and k^*_{off} (the steady-state and initial rate assumptions should apply over the time period during which the binding assay is run, see Note 1). Alternatively, the X block and X_1 subblock may also represent transport cycles that either work under steady-state conditions during the binding assay or have reached equilibrium at its start, so that all the reactions at the right of the inhibitor binding step would occur out of such transport cycles (see examples given in the Appendix). Accordingly, mechanisms A and B in Fig. 2 may also apply to slow-binding situations on the steady-state time scale as formally demonstrated below.

Let us assume in Fig. 2 *A* and *B*, that a product P can be generated from any number of N_i^X species with rate constant $(k_{cat})_i$, so that the rate of product formation can be expressed as

$$\frac{dP}{dt} = \sum_i (k_{cat})_i N_i^X = X \sum_i (k_{cat})_i f_i^X, \quad (53)$$

where $f_i^X = N_i^X/X$ represents the fractional concentrations of the product-generating N_i^X species. Substituting the time-dependent expression shown in Eq. 18 for X in Eq. 53 and integrating over time leads to

$$P = \sum_i (k_{cat})_i f_i^X \left[X_e t + \frac{X_0 - X_e}{k_{obs}} (1 - e^{-k_{obs}t}) \right], \quad (54)$$

in which $X_0 = N_T$ for both mechanisms A and B (Eq. 23), X_e is given by Eq. 19 in which Y_e is equivalent to B_e with algebraic expressions shown in Tables 1 and 2, and k_{obs} can be found from Eq. 13 and Table 1. Because the quantities

$$v_0 = \sum_i (k_{cat})_i f_i^X X_0 \quad (55)$$

and

$$v_e = \sum_i (k_{cat})_i f_i^X X_e \quad (56)$$

clearly represent, respectively, the initial velocity and the final steady-state velocity of product formation in the presence of inhibitor, Eq. 54 is fully equivalent to

$$P = v_s t + \frac{v_0 - v_s}{k_{obs}} (1 - e^{-k_{obs}t}), \quad (57)$$

which is the most general equation used to analyze burst kinetics of product formation in the steady-state approach (Morrison and Walsh, 1988). Accordingly, the linear and Michaelis–Menten forms of the k_{obs} versus $[I]$ plots demonstrated herein for mechanisms A and B, respectively, fully agree with the similar dependencies on $[I]$ previously reported for this parameter using elementary counterparts of these kinetic schemes (Morrison and Walsh, 1988). Note, then, that our studies extend these previous conclusions to almost any kinetic scheme and to inhibitors other than competitive, provided that Eqs. 50 (mechanism B) or 52 (mechanism A) can be applied to a specific kinetic mechanism.

Relevance of mechanism C to slow-binding inhibitors

To our knowledge, mechanism C depicted in Fig. 2 has never been analyzed in the context of enzyme kinetics and may not apply to catalytic systems that demonstrate linear reaction rates. Indeed, the presence of a slow isomerization step is reminiscent of a property usually associated with hysteretic enzymes, which can demonstrate more complex behavior (Neet and Ainslie, 1980). In contrast, the analogy between mechanism C and the recruitment hypothesis (Aronson, 1978) is quite obvious because the extent of inhibitor binding in block Y_2 is conditioned by the rate-

limiting recruitment of the N_i^X species into block *Y*. However, if mechanism C is meant to represent a transport process, the slow isomerization step should be part of the transport cycle itself, which raises the question of its relevance to slow-binding inhibition.

As noted earlier (see Materials and Methods and Results sections), there is a marked difference among the models A–C depicted in Fig. 2 in that at least part of the inhibitor molecules bound to the protein in models A and B would be protected by the rate-limiting step from free exchange with either the inhibitor itself or the natural substrate, should these be added to the incubation medium. Accordingly, debinding of the inhibitor should always be fast in mechanism C under these conditions. For the very same reason, inhibitor binding may not even be measurable using a radiotracer technique in combination with a rapid filtration assay because fast debinding during the washing steps would be expected with this type of mechanism. Quite obviously, then, these considerations cast doubt on the hypothesis that slow phlorizin binding to the Na^+-D-glucose cotransporter(s) is due to rate limiting by the free-carrier recycling step (Aronson, 1978; Toggenburger et al., 1978, 1982; Turner and Silverman, 1981; Restrepo and Kimmich, 1986). In fact, the validity of the recruitment hypothesis can be assessed directly. As shown in the Appendix, where mechanism C is considered in relation to the two most relevant mechanisms of Na^+-D-glucose cotransport proposed to date (Parent et al., 1992b; Kimmich, 1990; Chen et al., 1997), the k^*_{on} value for binding of a competitive inhibitor should, at best, be equal to that estimated for the turnover number of the catalytic process (k_{cat}) using the natural substrate under symmetrical conditions. Because Eq. 13 also applies, this is to state that the $t_{1/2}$ for binding should always be less than the $t_{1/2}$ required to perform one catalytic cycle in this type of mechanisms. Accordingly, with a turnover number of 5–125 catalytic cycles of Na^+-glucose cotransport per second (Kimmich, 1990), it can be concluded that equilibrium binding of phlorizin should be reached in the subsecond time range and that the recruitment hypothesis does not apply to SGLT1.

Relevance of mechanisms A and B to the fast-acting slow-binding paradigm

As discussed in the Introduction, the fast-acting slow-binding paradigm results from the apparent contradiction between observations originating from the parallel application of the general and direct approaches to the analysis of protein-inhibitor interactions in a given system. The fast-acting behavior seen with the general approach does call into question the assumption that the steady-state approach is valid for resolving the slow kinetics of inhibitor binding observed with the direct approach, but also rules out mechanism A as a possible explanation of the slow-binding kinetics (see Note 3).

Because neither mechanism A nor mechanism C may explain the fast-acting slow-binding paradigm of phlorizin, then mechanism B should represent the only alternative solution. Indeed, the restrictive 0–9-s time range over which the steady-state kinetics of glucose transport can be assessed in the absence of inhibitor (Chenu and Berteloot, 1993; Oulianova and Berteloot, 1996) may preclude the observation of burst kinetics in its presence because full equilibration of phlorizin binding requires several minutes (Glossmann and Neville, 1972; Chesney et al., 1974; Aronson, 1978; Turner and Silverman, 1981; Koepsell et al., 1990). Accordingly, the steady-state inhibition of transport activity may just be apparent and would mostly reflect the rapid formation of the initial collision complex. Moreover, because the inhibitor binding assay in these studies involves a rapid filtration technique coupled with the use of radioactive phlorizin, the fast dissociation rates associated with the initial collision complex could lead to a fast wash out of the inhibitor molecules bound to this complex during the washing steps in this experimental design. Accordingly, the slow kinetics of inhibitor binding would essentially characterize the slow isomerization of the initial collision complex into a more stable form, in conformity with the predictions of mechanism B (occluded) (Tables 1 and 2).

In addition to these theoretical and experimental considerations, there are a number of related results with regard to phlorizin binding that still remain to be satisfactorily explained: 1) the K_i value for glucose transport inhibition in rabbit kidney vesicles, $\approx$15 μM as determined by Oulianova and Berteloot (1996) or recalculated by these authors from the data of Turner and Moran (1982a), appears close to one order of magnitude higher than the K_d value of phlorizin binding measured at equilibrium (1.7–1.9 μM) in similar preparations (Turner and Moran, 1982b); 2) in rabbit intestinal vesicles, the apparent K_i value for glucose transport inhibition decreased from 40–50 μM when measured at 0.1 s to approx. 7 μM when estimated over the time interval 1.3–1.8 s (Toggenburger et al., 1982); and 3) in *Xenopus laevis* oocytes overexpressing the rabbit SGLT1 clone, the K_i value of $\approx$30 μM for phlorizin blockade of the presteady-state current (Hazama et al., 1997) appears significantly higher than the K_i value of 2–10 μM for phlorizin inhibition of the sugar-induced steady-state current (Wright, 1993). Interestingly, all of these observations seem to agree that the apparent affinity for phlorizin binding may increase with time, a behavior that can be interpreted as strong evidence in support of mechanism B (Eq. 48). Still, a final conclusion to this matter may have to await direct demonstration that the kinetics of phlorizin binding do follow those expected for mechanism B.

APPENDIX: RELATIONSHIP BETWEEN THE APPARENT FIRST-ORDER RATE OF INHIBITOR BINDING (k_{obs}) AND THE TURNOVER NUMBER FOR SUBSTRATE TRANSPORT (k_{cat}) IN THE RECRUITMENT HYPOTHESIS (MECHANISM C)

The kinetics of phlorizin binding to the SGLT proteins of renal and intestinal membranes have previously been inter-

preted according to the recruitment concept (Mechanism C in Fig. 2), whereby the rate-limiting step in the binding process is designated by the free-carrier recycling step while the different carrier species are in equilibrium with the ligands at the two membrane faces (Aronson, 1978; Turner and Silverman, 1980). The purpose of this appendix is to demonstrate that the validity of the recruitment hypothesis is dependent on the turnover number for transport measured under symmetrical conditions using the natural substrate.

No consensus has yet been reached as to the order of Na^+ and substrate (inhibitor) addition on the SGLT1 protein, and Fig. A1 depicts the two most relevant mechanisms proposed to date. The N:N:S model (Fig. A1 *A*) was originally proposed by Parent et al. (1992b) and assumes that the binding of the two Na^+ ions to the transport protein can be described as a single reaction step that precedes substrate (inhibitor) addition, a hypothesis that has since been shown to be compatible with strong cooperativity for Na^+ binding (Falk et al., 1998). The N:S:N model (Fig. A1 *B*), in which the substrate (inhibitor) binding step occurs between the two Na^+ binding events, has been advocated by Kimmich's lab (Kimmich, 1990) and has received support in a recent paper by Chen et al. (1997). Note that these two mechanisms are presented in Fig. A1 to satisfy the rapid equilibrium assumption inherent to the recruitment hypothesis, and that they have in common a Na^+ leak pathway (N_3 to N_4 transition) for which evidence has been provided by Parent et al. (1992a) and by Chen et al. (1997) for the N:N:S and N:S:N models, respectively. We do not intend to discuss here the pros and the cons for the two schemes but, rather, to demonstrate that the same conclusion may apply to both.

The rapid equilibrium assumption allows us to define the two blocks of elementary reactions called X and Y in Fig. A1 to emphasize the similarities with model C in Fig. 2. As discussed in the text, it is possible to reduce both mechanisms to the same elementary scheme shown in Fig. 1 *B* using Cha's formalism (Cha, 1968), and thus to use Eqs. 50 and 51 to write down the equalities

$$k^*_{on} = k_{12}f_1 + k_{43}f_4, \tag{A1}$$

$$k^*_{off} = k_{21}f_2 + k_{34}f_3. \tag{A2}$$

Note that the numbering of the carrier species was chosen in such a way that Eqs. A1 and A2 may apply to both of the situations depicted in Fig. A1. The f_i fractions can be calculated as proposed in the text or with the help of a computer program (Falk et al., 1998); the relevant algebraic expressions are given in Table A1, as well as those of k^*_{on} and k^*_{off} that result from proper substitutions into Eqs. A1 and A2, and from a few arithmetic rearrangements thereafter. As predicted for mechanism C in Fig. 2 and its associated kinetic features reported in Table 1, only k^*_{off} is affected by the inhibitor concentration and the value of this parameter decreases to zero at saturation. Because Eq. 13 also applies, the k^*_{on} value represents the smallest possible value for k_{obs} (i.e., the slowest rate of binding that may be

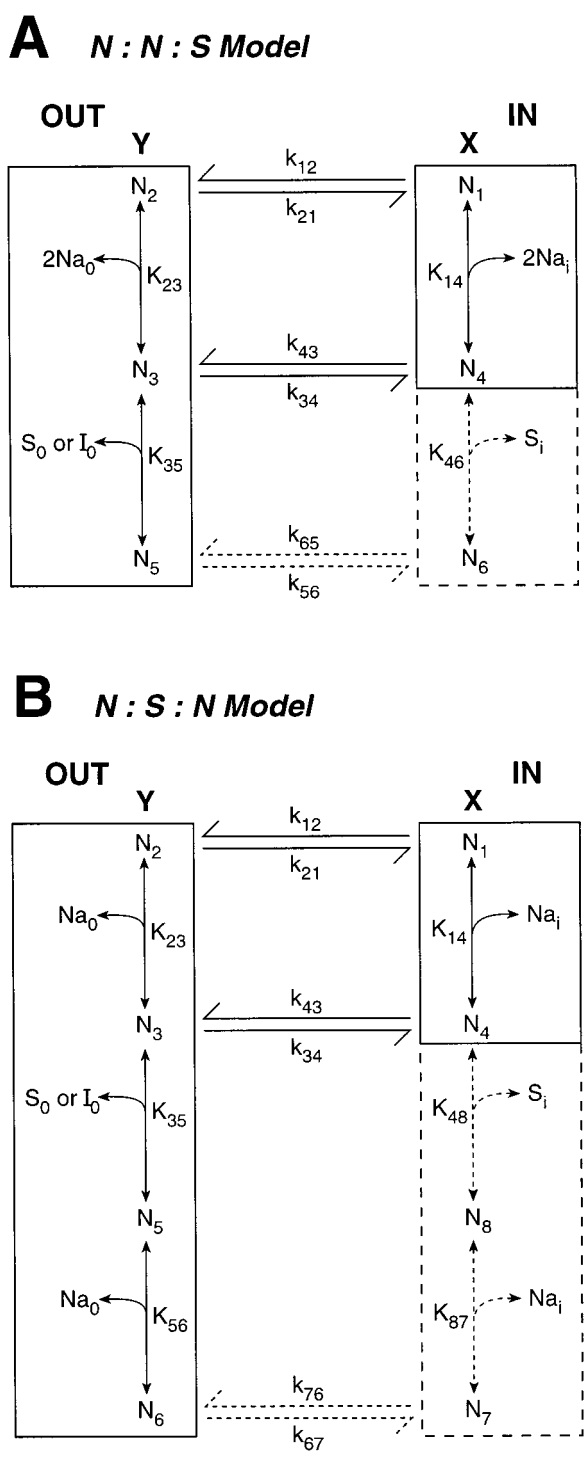

FIGURE A1 Kinetic mechanisms of Na^+-D-glucose cotransport. (*A*) The N:N:S model proposed by Parent et al. (1992b), in which the binding of the two Na^+ ions to the transport protein is depicted as a single reaction step that precedes phlorizin (I) or glucose (S) addition. (*B*) The N:S:N model proposed by Chen et al. (1997) in which the I or S binding step comes between the two Na^+ binding events. In both A and B, the full line represents the elementary reactions and the blocks that need to be considered to describe phlorizin binding. The extra reactions and block extensions in dashed lines should also be included to account for glucose transport. The indices i and o associated with the effectors refer, respectively, to the internal (IN) and external (OUT) location of these effectors relative to their binding sites on the transport protein. The naming of the X and Y blocks was chosen to emphasize the similarity of these models with mechanism C in Fig. 2.

TABLE A1 Algebraic expressions of the f_i fractions characterizing the N_i species involved in the relaxation process, and of the apparent first-order rates for inhibitor association to (k^*_{on}) and dissociation from (k^*_{off}) the transporter

	Kinetic Mechanisms	
Parameters	N:N:S model (Fig. A1 *A*)	N:S:N model (Fig. A1 *B*)
f_1	K_{14}/D^X	K_{14}/D^X
f_2	$K_{23}K_{35}/D^Y$	$K_{23}K_{35}K_{56}/D^Y$
f_3	$K_{35}(Na_o)^2/D^Y$	$K_{35}K_{56}(Na_o)/D^Y$
f_4	$(Na_i)^2/D^X$	$(Na_i)/D^X$
k^*_{on}	$[k_{12}K_{14}+k_{43}(Na_i)^2]/D^X$	$[k_{12}K_{14}+k_{43}(Na_i)]/D^X$
k^*_{off}	$\{K_{35}[k_{21}K_{23}+k_{34}(Na_o)^2]\}/D^Y$	$\{K_{35}K_{56}[k_{21}K_{23}+k_{34}(Na_o)]\}/D^Y$
D^X	$K_{14}+(Na_i)^2$	$K_{14}+(Na_i)$
D^Y	$K_{35}[K_{23}+(Na_o)^2]+(Na_o)^2(I_o)$	$K_{35}K_{56}[K_{23}+(Na_o)]+[K_{56}+(Na_o)](Na_o)(I_o)$

The f_i fractions are defined as the N_i/X or N_i/Y ratios where X and Y represent $\Sigma_i N_i$ in blocks X and Y in Fig. A1 with algebraic expressions as given by the temporary constants D^X and D^Y. All the other constants and symbols are explicitly defined in Fig. A1.

achieved). The comparison between k^*_{on} and the turnover rate of substrate transport (k_{cat}) may thus prove necessary and sufficient to predict the time scale over which the kinetics of inhibitor binding may be observed in a realistic experiment.

Both phlorizin binding and glucose transport studies have usually been performed with membrane vesicles (Aronson, 1978; Chesney et al., 1974; Glossmann and Neville, 1972; Koepsell et al., 1990; Toggenburger et al., 1978, 1982; Turner and Moran, 1982b; Turner and Silverman, 1981) or epithelial cells (Moran et al., 1988; Restrepo and Kimmich, 1986) in the complete absence of internal substrate while the Na^+ concentration was varied in both the external and internal media. To perform the comparison detailed above, one may only need to establish the algebraic expression of k_{cat} under initial rate conditions of transport when $S_i = 0$. This is most easily done by first deriving the velocity equations relative to substrate transport (v_i^S) using a computer program (Falk et al., 1998) with resultant Eqs. A3 and A4,

$$\frac{v_i^S}{N_T} = \frac{[C_1 + C_2(Na_i)^2](Na_o)^2(S_o)}{C_3 + C_4(Na_i)^2 + [C_5 + C_6(Na_i)^2](Na_o)^2, + [C_7 + C_8(Na_i)^2](Na_o)^2(S_o)} \quad \text{(A3)}$$

$$\frac{v_i^S}{N_T} = \frac{[C_1 + C_2(Na_i)](Na_o)^2(S_o)}{C_3 + C_4(Na_i) + [C_5 + C_6(Na_i)](Na_o), + \{C_7 + C_8(Na_i) + [C_9 + C_{10}(Na_i)](Na_o)\}(Na_o)(S_o)} \quad \text{(A4)}$$

for the N:N:S and N:S:N models, respectively, in which the algebraic expressions of the macro constants (C_i) are given in Table A2. Because

$$k_{cat} = \frac{V_{max}}{N_T}, \quad \text{(A5)}$$

where V_{max} represents the apparent maximum rate of transport, k_{cat} can be obtained from Eqs. A3 and A4 by dividing the (S_o) coefficient term in the numerator by the (S_o) coefficient term in the denominator, which results in the algebraic expressions of k_{cat} shown in Table A2 following proper substitutions and calculations. With the factorization used to report the algebraic expressions of k^*_{on} and k_{cat} in Tables A1 and A2, it is readily apparent that the k^*_{on}/k_{cat} ratio can be cast in the forms

$$\frac{k^*_{on}}{k_{cat}} = 1 + \frac{k_{12}K_{14} + k_{43}(Na_i)^2}{k_{56}[K_{14} + (Na_i)^2]} \geq 1, \quad \text{(A6)}$$

TABLE A2 Algebraic expressions of the macro constants (C_i) appearing in the initial velocity Eqs. A3 and A4, and of the turnover number (k_{cat}) for substrate transport

	Kinetic Mechanisms	
Constants	N:N:S model (Fig. A1 *A*)	N:S:N model (Fig. A1 *B*)
C_1	$k_{12}k_{56}K_{14}$	$k_{12}k_{67}K_{14}$
C_2	$k_{43}k_{56}$	$k_{43}k_{67}$
C_3	$(k_{12} + k_{21})K_{14}K_{23}K_{35}$	$(k_{12} + k_{21})K_{14}K_{23}K_{35}K_{56}$
C_4	$(k_{21} + k_{43})K_{23}K_{35}$	$(k_{21} + k_{43})K_{23}K_{35}K_{56}$
C_5	$(k_{12} + k_{34})K_{14}K_{35}$	$(k_{12} + k_{34})K_{14}K_{35}K_{56}$
C_6	$(k_{34} + k_{43})K_{35}$	$(k_{34} + k_{43})K_{35}K_{56}$
C_7	$(k_{12} + k_{56})K_{14}$	$k_{12}K_{14}K_{56}$
C_8	$k_{43} + k_{56}$	$k_{43}K_{56}$
C_9	—	$(k_{12} + k_{67})K_{14}$
C_{10}	—	$k_{43} + k_{67}$
k_{cat}	$\frac{k_{56}[k_{12}K_{14} + k_{43}(Na_i)^2]}{k_{56}[K_{14} + (Na_i)^2] + k_{12}K_{14} + k_{43}(Na_i)^2}$	$\frac{k_{67}[k_{12}K_{14} + k_{43}(Na_i)](Na_o)}{k_{67}(Na_o)[K_{14} + (Na_i)] + [K_{56} + (Na_o)][k_{12}K_{14} + k_{43}(Na_i)]}$

The algebraic expressions of k_{cat} were calculated as described in the text. All the other constants and symbols are explicitly defined in Fig. A1.

$$\frac{k^*_{on}}{k_{cat}} = 1 + \frac{[K_{56} + (Na_o)][k_{12}K_{14} + k_{43}(Na_i)]}{k_{67}(Na_o)[K_{14} + (Na_i)]} \geq 1, \quad \text{(A7)}$$

for the N:N:S and N:S:N models, respectively. Accordingly, the time course of phlorizin binding should proceed over a time scale that is at best equivalent to that required to perform one catalytic cycle of glucose transport or, to state otherwise, equilibrium binding of the inhibitor should have been reached at a time when steady-state kinetics of glucose transport are observed. In the particular case of SGLT1, for which a turnover number of 5–125 catalytic cycles per second has been reported under a large spectrum of experimental conditions (Kimmich, 1990), equilibrium binding of phlorizin should thus be attained in the subsecond time range, hence the conclusion in the main text that the recruitment hypothesis does not apply to SGLT1. For both the N:N:S and N:S:N models, note that this conclusion is independent of whether or not there is a Na^+ leak pathway ($k_{43} = 0$ in Eqs. A6 and A7) and that, in the absence of such a pathway, saturating concentrations of internal Na^+ leads to $k^*_{on} = k_{cat}$.

NOTES

1. The substrate concentration can be regarded as constant while the product concentration remains sufficiently low, so that the steady-state distribution of the different enzyme species is not affected by substrate depletion or product formation and the reverse reaction is insignificant.

2. If the rates of inhibitor association with and dissociation from the protein are fast in mechanism A, or if the forward and reverse isomerization rates associated with mechanism B are relatively high, the change in going from the initial to the final steady-state rate could be rapid and essentially undetectable by these procedures.

3. Should mechanism A apply to such situations, the tested compound may fail to reveal itself as an inhibitor of the reaction under study (there is not enough EI complex formed during velocity measurements to significantly inhibit the enzyme reaction). Similarly, in mechanism B, a molecule with the properties of a slow-binding inhibitor may appear to behave as a classical inhibitor (only the rapidly formed initial collision complex would significantly contribute to enzyme inhibition during velocity measurements).

4. Indeed, binding of a fast-acting inhibitor should be complete by the time steady-state rates of catalytic reactions are measured. By contrast, the time constant accounting for the binding of slow-binding inhibitors should be identical to that describing the burst kinetics of the catalytic reaction under symmetrical conditions.

5. Note that the observation of monoexponential kinetics under pre-steady-state conditions may not easily be achieved in the presence of many effectors, some of which may bind to and dissociate from the protein at very similar rates. However, the experimental conditions may be worked out to isolate part of a reaction sequence that may be reduced to the basic schemes shown in Fig. 2, in which *I* may now stand for any type of effector involved in the reaction sequence.

6. To compare the present analyses and the previous studies of Wierzbicki et al. (1990), note that Table 4 in the latter article reports the algebraic expressions of $1/\alpha$ and that the parameter α is equivalent to k_{obs} in the former.

The authors thank C. Gauthier for the art work, and Drs. M. C. Coady, C. Jumarie, and J.-Y. Lapointe for careful reading of the manuscript and suggestions for improvement. This research was supported by grant MT-14407 from the Medical Research Council of Canada.

REFERENCES

Aronson, P. 1978. Energy-dependence of phlorizin binding to isolated renal microvillus membranes. *J. Membr. Biol.* 42:81–98.

Berteloot, A., C. Malo, S. Breton, and M. Brunette. 1991. A fast-sampling, rapid-filtration apparatus: principal characteristics and validation from studies of D-glucose transport in human jejunal brush-border membrane vesicles. *J. Membr. Biol.* 122:111–125.

Berteloot, A., and G. Semenza. 1990. Advantages and limitations of vesicles for the characterization and the kinetic analysis of transport systems. *Methods Enzymol.* 192:409–437.

Cha, S. 1968. A simple method for derivation of rate equations for enzyme-catalyzed reactions under the rapid equilibrium assumption or combined assumptions of equilibrium and steady state. *J. Biol. Chem.* 243:820–825.

Chen, X.-Z., M. J. Coady, F. Jalal, B. Wallendorff, and J.-Y. Lapointe. 1997. Sodium leak pathway and substrate binding order in the Na^+-glucose cotransporter. *Biophys. J.* 73:2503–2510.

Chenu, C., and A. Berteloot. 1993. Allosterism and Na^+-D-glucose cotransport kinetics in rabbit jejunal vesicles: compatibility with mixed positive and negative cooperativities in a homodimeric or tetrameric structure and experimental evidence for only one transport protein involved. *J. Membr. Biol.* 132:95–113.

Chesney, R., B. Sacktor, and A. Kleinzeller. 1974. The binding of phlorizin to the isolated luminal membrane of the renal proximal tubule. *Biochim. Biophys. Acta.* 332:263–277.

Diedrich, D. F. 1966. Competitive inhibition of intestinal glucose transport by phlorizin analogs. *Arch. Biochem. Biophys.* 117:248–256.

Falk, S., A. Guay, C. Chenu, S. D. Patil, and A. Berteloot. 1998. Reduction of an eight-state mechanism of cotransport to a six-state model using a new computer program. *Biophys. J.* 74:816–830.

Glossmann, H., and D. M. Neville, Jr. 1972. Phlorizin receptors in isolated kidney brush border membranes. *J. Biol. Chem.* 247:7779–7789.

Hazama, A., D. D. Loo, and E. M. Wright. 1997. Presteady-state currents of the rabbit Na^+/glucose cotransporter (SGLT1). *J. Membr. Biol.* 155: 175–186.

Kimmich, G. A. 1990. Membrane potential and the mechanism of intestinal Na^+-dependent sugar transport. *J. Membr. Biol.* 114:1–27.

Koepsell, H., G. Fritzsch, K. Korn, and A. Madrala. 1990. Two substrate sites in the renal Na^+-D-glucose cotransporter studied by model analysis of phlorizin binding and D-glucose transport measurements. *J. Membr. Biol.* 114:113–132.

Moran, A., L. J. Davis, and R. J. Turner. 1988. High affinity phlorizin binding to the LLC-PK_1 cells exhibits a sodium:phlorizin stoichiometry of 2:1. *J. Biol. Chem.* 263:187–192.

Morrison, J. F., and C. T. Walsh. 1988. The behavior and significance of slow-binding enzyme inhibitors. *Adv. Enzymol.* 61:201–301.

Neet, K. E., and Ainslie, G. R., Jr. 1980. Hysteretic enzymes. *Methods Enzymol.* 64:192–226.

Oulianova, N., and A. Berteloot. 1996. Sugar transport heterogeneity in the kidney: two independent transporters or different transport modes through an oligomeric protein? I. Glucose transport studies. *J. Membr. Biol.* 153:181–194.

Parent, L., S. Supplisson, D. D. F. Loo, and E. M. Wright. 1992a. Electrogenic properties of the cloned Na^+/glucose cotransporter. I. Voltage-clamp studies. *J. Membr. Biol.* 125:49–62.

Parent, L., S. Supplisson, D. D. F. Loo, and E. M. Wright. 1992b. Electrogenic properties of the cloned Na^+/glucose cotransporter. II. A transport model under nonrapid equilibrium conditions. *J. Membr. Biol.* 125:63–79.

Restrepo, D., and G. A. Kimmich. 1986. Phlorizin binding to isolated enterocytes: membrane potential and sodium dependence. *J. Membr. Biol.* 89:269–280.

Schwartz, A., G. E. Lindenmayer, J. C. Allen, and J. L. McCans. 1974. The nature of the cardiac glycoside enzyme complex: mechanism and kinetics of binding and dissociation using a high-activity heart Na^+, K^+-ATPase. *Proc. Natl. Acad. Sci. USA.* 242:577–597.

Sculley, M. J., J. F. Morrison, and W. W. Cleland. 1996. Slow-binding inhibition: the general case. *Biochim. Biophys. Acta.* 1298:78–86.

Semenza, G., M. Kessler, M. Hosang, J. Weber, and U. Schmidt. 1984. Biochemistry of the Na^+-D-glucose cotransporter of the small intestine brush-border membrane: the state of the art in 1984. *Biochim. Biophys. Acta.* 779:343–379.

Toggenburger, G., M. Kessler, A. Rothstein, G. Semenza, and C. Tannenbaum. 1978. Similarity in effects of Na^+ gradients and membrane potentials on D-glucose transport by, and phlorizin binding to, vesicles derived from brush borders of rabbit intestinal mucosal cells. *J. Membr. Biol.* 40:269–290.

Toggenburger, G., M. Kessler, and G. Semenza. 1982. Phlorizin as a probe of the small-intestinal Na^+, D-glucose cotransporter: a model. *Biochim. Biophys. Acta.* 688:557–571.

Turner, R. J., and A. Moran. 1982a. Heterogeneity of sodium-dependent D-glucose transport sites along the proximal tubule: evidence from vesicle studies. *Am. J. Physiol.* 242:F406–F414.

Turner, R. J., and A. Moran. 1982b. Further studies of proximal tubular brush border membrane D-glucose transport heterogeneity. *J. Membr. Biol.* 70:37–45.

Turner, R. J., and M. Silverman. 1980. Testing carrier models of cotransport using the binding kinetics of non-transported competitive inhibitors. *Biochim. Biophys. Acta.* 596:272–291.

Turner, R. J., and M. Silverman. 1981. Interaction of phlorizin and sodium with the renal brush-border membrane D-glucose transporter: stoichiometry and order of binding. *J. Membr. Biol.* 58:43–55.

Volkenstein, M. V., and B. N. Goldstein. 1966. A new method for solving the problem of the stationary kinetics of enzymological reactions. *Biochim. Biophys. Acta.* 115:471–477.

Wierzbicki, W., A. Berteloot, and G. Roy. 1990. Presteady-state kinetics and carrier-mediated transport: a theoretical analysis. *J. Membr. Biol.* 117:11–27.

Wright, E. M. 1993. The intestinal Na^+/glucose cotransporter. *Annu. Rev. Physiol.* 55:575–589.